Flexibility within Myosin Heads Revealed by Negative Stain and Single-Particle Analysis

S.A. Burgess,* M.L. Walker,* H.D. White,‡ and J. Trinick*

*Department of Clinical Veterinary Sciences, University of Bristol, Langford, Bristol, BS18 7DY, United Kingdom; and
‡Biochemistry Department, Eastern Virginia Medical School, Norfolk, Virginia 23507

Abstract. Electron microscopy of negatively stained myosin has previously revealed three discrete regions within the heads of the molecule. However, despite a probable resolution of ~2 nm, it is difficult to discern directly consistent details within these regions. This is due to variability in both head conformation and in staining. In this study, we applied single-particle image processing and classified heads into homogeneous groups. The improved signal-to-noise ratio after averaging these groups reveals substantially improved detail. The image averages were compared to a model simulating negative staining of the atomic structure of subfragment-1 (S1). This shows that the three head regions correspond to the motor domain and the essential and regulatory light chains. The image averages were very similar to particular views of the S1 model. They also revealed considerable flexibility between the motor and regulatory domains, despite the molecules having been prepared in the absence of nucleotide. This flexibility probably results from rotation of the regulatory domain about the motor domain, where the relative movement of the regulatory light chain is up to 12 nm, and is most clearly illustrated in animated sequences (available at http://www.leeds.ac.uk/chb/muscle/myosinhead.html). The sharply curved conformation of the atomic model of S1 is seen only rarely in our data, with straighter heads being more typical.

Muscle force is derived from the interaction of myosin and actin. The most likely mechanisms involve a large conformational change in the attached head of the myosin molecule, either in the binding angle made with actin (Huxley, 1969), or within the head itself (Rayment et al., 1993*a*). Attached heads may also deform elastically in response to stress, allowing storage of strain energy derived from ATP or stretching. Information about the structure and flexibility of the myosin head is therefore important in exploring the molecular mechanism of force generation.

The most detailed electron micrographs of myosin molecules have been obtained by negative staining and have revealed three discrete regions within the heads. The most common appearance consists of a large distal region connected to the head–tail junction by two smaller regions in line (Walker et al., 1985; Walker and Trinick, 1986, 1988). After the subsequent elucidation of the atomic structure of myosin subfragment-1 (S1)[1] by X-ray crystallography (Rayment et al., 1993*b*), it seemed likely that the three regions identified correspond to the motor domain and the essential and regulatory light chains. However, although the micrographs show many details, probably to a resolution of ~2 nm, further analysis is hindered by the wide variations in head appearance and by the considerable noise caused by the size and variability of the stain crystallites.

It is possible to recover more information from such micrographs by using the image processing technique known as "single-particle analysis" (Frank, 1996). This allows images with similar appearances to be classified into homogeneous groups; these can then be averaged, thus improving the signal-to-noise ratio. This type of approach was used previously with the heads of shadowed myosin molecules (Vibert, 1988). Here we describe its application to negatively stained molecules, which reveals a considerable amount of new detail. To confirm the validity of our results we developed a negative stain model and simulated staining of the atomic structure of S1. This showed that the three regions in stained myosin heads are indeed the motor domain and the essential and regulatory light chains (the regulatory domain).

Initial attempts to classify the images based on the appearances of whole heads were difficult to interpret. It emerged that heads not only adopt a variety of orientations on the grid, but also a variety of conformations be-

Address all correspondence to J. Trinick, at his current address, Department of Human Biology, Leeds University, Leeds LS2 9JT, United Kingdom. Tel.: 44-113-233-4350. Fax: 44-113-233-4344. E-mail: j.trinick@leeds.ac.uk

1. *Abbreviation used in this paper*: S1, subfragment 1.

tween the motor and regulatory domains. Single particle analysis has been used previously, mainly with invariant structures. Therefore, we classified heads twice: first using only the motor domains, and then using only the regulatory domains. The data from both rounds of classification were then combined. The results demonstrate a large degree of flexibility within heads.

Materials and Methods

Specimen Preparation

Negative staining of myosin was carried out as described previously (Walker et al., 1985; Walker and Trinick, 1986). Rabbit myosin, purified as described by Perry (1955), was diluted with 0.6 M Na-acetate, 5 mM $MgCl_2$, 1 mM EGTA, and 6 mM K-phosphate, pH 7.0, to a final concentration of ~4 μg/ml and applied to carbon-coated electron microscope grids. The films were prepared by resistive evaporation from carbon fibers onto freshly cleaved mica. Immediately before application of myosin, grids were irradiated for 40 min with a UV mercury vapor lamp (type R51; UV Products Inc., Pasadena, CA). The carbon was as thin as possible without being unacceptably fragile after the UV irradiation. Once on the grid, the myosin was washed with dilution buffer at 37°C before being stained with freshly prepared 1% uranyl acetate at 4°C (Walker and Trinick, 1986).

Electron Microscopy and Digitization

Grids were examined with an electron microscope (EM400T; Philips Electron Optics, Eindhoven, The Netherlands) operating at a magnification of ×46,000, and with a cold trap. A moderate dose (~10^5 electrons/nm^2) was used, but this was not accurately controlled. Whole micrographs were digitized as 16-bit images using a Leafscan-45 densitometer (Leaf Systems, Inc., Southborough, MA) with a pixel size corresponding to 0.435 nm. These data were then imported into the SPIDER program suite (Health Research Inc., Rensselaer, NY) (Frank et al., 1981*a*) running on a Silicon Graphics Indigo workstation (Silicon Graphics Computer Systems, Mountain View, CA). All subsequent image processing was performed using SPIDER.

Particle Selection and Alignment

Myosin molecules, showing at least one clearly visible head, were selected interactively and windowed out as 128 × 128 pixel images; these were large enough to contain both heads and a small portion of the tail. This selection from the original micrographs reduced the data from ~830 to ~100 megabytes. The digitized images were then scaled to adjust their pixel values to a mean of 0 ± 1.0 SD. Individual heads, which would constitute the single particles in the analysis, were then windowed interactively as 64 × 64 pixel images and brought into approximate alignment by programs using reference-free alignment (Penczek et al., 1992). Images found to have been misaligned were discarded: rotational misalignments by 180° were identified visually and particles requiring translational vectors of 16 pixels or more (~7 nm) were automatically removed. The alignment was then refined based on features within the motor domains. After this, images with rotations >±50° or shift vectors >6 pixels (~3 nm) were also discarded.

Classification of Heads

The aligned heads were low pass filtered to 1/2.0 nm^{-1} and classified directly (i.e., without prior treatments, such as correspondence analysis or principal components analysis) using "K-means clustering" (Frank, 1990) as follows. The data were classified in two independent rounds, using different masks to isolate the motor and regulatory domains. Thus each head was assigned to a particular motor domain and regulatory domain group. These two sets of results were then combined to produce a table in which each entry contained heads with consistent motor and regulatory domain appearances. All heads assigned to the same motor domain and regulatory domain subgroup were therefore similar in appearance and were averaged.

Negative Stain Model

To examine whether the new details revealed by image processing reflect the real structure of the head, we constructed a simple negative stain model using the atomic structure of chicken S1 (Rayment et al., 1993*b*). Firstly, a SPIDER volume was generated from the C^{α} atom coordinates of the atomic structure, with the amino acids represented by uniform density spheres of 0.6 nm diam. Cavities within this structure smaller than 2 nm were filled, to simulate exclusion of the 2-nm diam stain crystallites. This was achieved by low pass filtering the volume to 1/2.0 nm^{-1}, followed by thresholding to create a second volume. Adding this to the original volume created a new volume in which all invaginations <2 nm had been filled, leaving protrusions unaffected.

This volume was then rotated to generate a quasi-uniform distribution of orientations (Penczek et al., 1994) on a "carbon film" at 10° angular increments. Negative stain was simulated by low pass filtering this volume (S1 structure and carbon film), followed by thresholding and contrast inversion. The "stained" volume was then projected in a direction perpendicular to the carbon film to simulate the negative stain image. Finally, model images with similar orientations (±20°) were aligned and averaged, to simulate the effect of image classification and averaging (see Results). These model views were then compared to the real group averages by inspection.

Resolution

Because myosin heads are attached to the flexible head–tail junction, estimating the resolution of the image averages by the differential phase residual method (Frank et al., 1981*b*) is difficult, due to the choice that must be made about the shape of the mask used to isolate the head. However, with various masks designed to exclude the head–tail junction to greater and lesser extents, estimates in the region of 2.5 nm were common (for the larger subgroup averages). This is typical for the negative staining method.

Results

Head Selection and Alignment

Negatively stained myosin molecules generally show two comma shaped heads attached to a long thin tail (Fig. 1). Flexibility about the head–tail junction is shown by the wide variety of head orientations (Fig. 2). Variations in head curvature and substructure are also evident.

1,512 such images were obtained from a data set comprising molecules stained in the absence of any nucleotide.

Figure 1. Examples of negatively stained myosin molecules prepared in the absence of nucleotide. The two heads and tail are clearly visible. Bar, 20 nm.

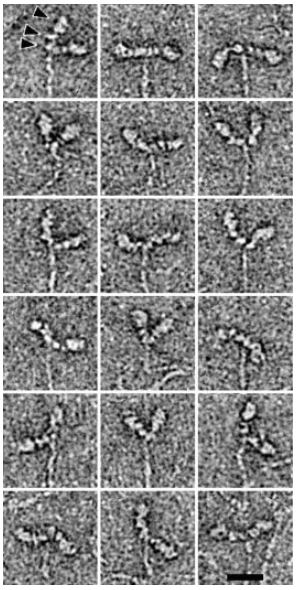

Figure 2. Gallery of typical myosin heads used in this study. The heads display various degrees of curvature and occasionally three discrete structural regions can be visualized (*arrowheads*). Individual heads were identified interactively from such images for use in the single-particle analysis. Bar, 20 nm.

From these images, 2,492 individual heads were selected and subjected to alignment. Removal of misaligned heads left 2,289 images after the first round of alignment. Because we were aware that the heads showed curvature and possibly flexibility, a second alignment was done using only the motor domain; after this refinement there were 1,951 heads in the data set. The average and variance images from both rounds of alignment are shown in Fig. 3. The reduction in variance around the motor domain in Fig. 3 *d* shows that the refinement was successful. Fig. 3 also shows the three head regions identified previously much more clearly than in the original micrographs (Walker et al., 1985; Walker and Trinick, 1988).

Negative Stain Model

The negative stain model is illustrated in Fig. 4. This shows how two different orientations of S1 are affected by simulated staining. In some orientations, part of S1 falls outside the stain envelope and so does not contribute to the final image (Fig. 4, *f–j*).

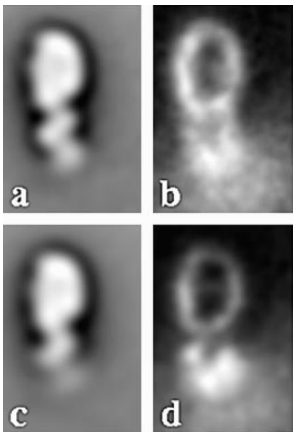

Figure 3. (*a*) Global average after the first round of alignment (n = 2,289). Despite the multitude of head appearances making up this image, three structural regions corresponding to the motor domain and both light chains are clearly visible. (*b*) Variance image from *a.* White indicates high variance. As is typical in negative stain images, most variability is in the periphery of the molecule where stain collects. (*c*) Global average of the heads after refinement (n = 1,951), and corresponding variance image (*d*). Note the reduction in variance around the motor domain and the increase in the region of the light chains.

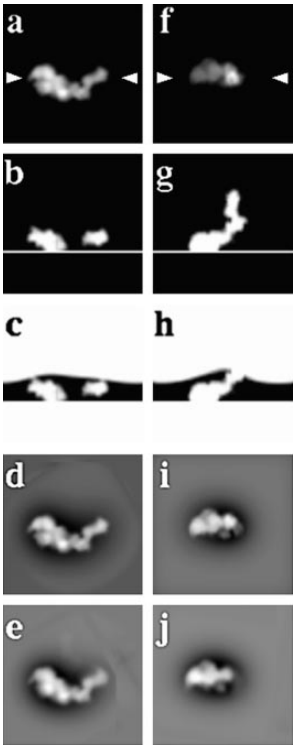

Figure 4. S1 modeled in negative stain. Two orientations of S1 are shown (*a–e*, and *f–j*). (*a*) Simple projections. Arrowheads (*a* and *f*) indicate the position of the sections shown in (*b* and *g*), made perpendicular to the carbon film (*b* and *g*, *white line*). (*c* and *h*) Negative stain envelopes. The relative electron densities of stain and protein were chosen to be 100:1. (*d* and *i*) Projections of "stained" S1. The regulatory light chain contributes very little to the image (*i*) because it falls outside the stain envelope. When images with similar orientations are aligned and averaged (*e* and *j*) there is a small degradation in the overall contrast of the images, and in particular, the regulatory light chain (*e*) becomes weaker.

The appearance of S1 in the model was relatively insensitive to the choice of parameters used to determine both the stain envelope profile and the relative electron densities of stain and protein (chosen as 100:1). However, the appearance was altered dramatically by the overall stain depth: this determined how much of the S1 structure fell within the stain envelope and also affected the contrast of protein, peripheral stain, and background stain in the final image. We chose a depth (3.7 nm; Fig. 4, *c* and *h*) that best reproduced the contrast in the real group averages (see Figs. 7 and 8).

Classification of Heads

Attempts to classify whole heads revealed that those with similar motor domain appearances possessed a variety of regulatory domain appearances. It therefore appeared that the motor and regulatory domains might be moving relative to one another. Since single particle analysis has mainly been used with invariant structures, we divided the classification into two stages, based separately on the motor and regulatory domains. Combining the results from both rounds of classification would allow us to demonstrate unequivocally that heads with the same motor domain appearance could display a variety of regulatory domain appearances. The masks used to isolate these regions of the heads are shown in Fig. 5.

It was also apparent that the data contained no distinct groups or clusters, which indicates there were no strongly preferred orientations on the grid. Thus, dividing the data into groups suitable for averaging was somewhat arbitrary and these would inevitably contain a range of orientations. Extensive tests were made with several different classification strategies, involving various combinations of correspondence analysis, principal components analysis, and hi-

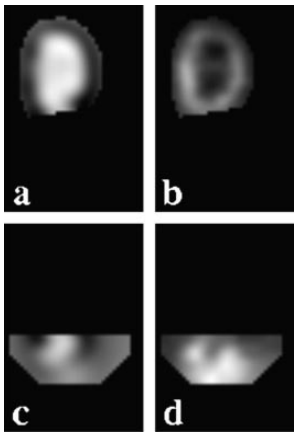

Figure 5. Masks used in image classification. (*a*) Refined average and (*b*) variance images masked to isolate the motor domains. The mask must be sufficiently large to contain all motor domain morphologies (indicated by the high variance), yet small enough to exclude as much of the background as possible. (*c*) Average and (*d*) variance images masked to isolate the regulatory domains.

erarchical ascendant classification, but these produced unsatisfactory results in the way individual images were merged into groups. Finally, we found that the technique known as K-means clustering was the most successful because it allowed us to control the division of the relatively uniformly distributed data into groups of roughly similar sizes. We examined the results of many trials, varying the number of groups between 2 and 60. In deciding on the optimum number, we needed to balance two conflicting trends: fewer groups contain more individual heads per group, thereby allowing a more detailed examination of their regulatory domains; whereas more groups can show greater morphological diversity. We found that 20 groups provided sufficient diversity, while maintaining large enough group sizes to enable a second classification into four regulatory domain subgroups.

The results of classification are shown in Fig. 6. Only those motor domain groups that compared favorably with the model are included (see below). Both the motor domains (Fig. 6, *top row*) and regulatory domains (Fig. 6, *left column*) show a surprising amount of detail, the essentials of which are preserved in their corresponding subaverages (where $n > 8$). Within each column, the appearance of the motor domains is constant, but the regulatory domains show considerable variability; this strongly suggests that head conformation is variable.

K-means clustering was repeated a number of times because the outcome can depend upon the initial choice of seeds used in the iterative process (Frank, 1996). However, the results were consistent from trial to trial and those presented in Fig. 6 are typical. Furthermore, heterogeneity of the regulatory domain was a consistent finding regardless of the number of motor domain groups chosen (up to 50, data not shown), although the improvement in signal-to-noise ratio in these was, of course, poorer.

Comparison between Data and Model

Rotating S1 in the model about a single axis at 36° intervals produced good matches with the regulatory domains in the data (Fig. 7). Thus the regulatory domains appear to be related to one another by rotation through an angle of about 110°. However, agreement with the motor domains was good in only some cases. This suggests that the motor and regulatory domains may also have rotated with respect to one another.

Good matches with the motor domains were found for 10 of the 20 group averages in the data (Fig. 8, *a* and *b*). From the model (Fig. 8 *b*) it is clear that the motor domain is highly asymmetric and different orientations account for many of the appearances seen in the data, even when the model images contain orientations within ±20°. A close match with the remaining 10 groups could not be found so we excluded them.

Having determined the approximate orientations of the motor domains, we combined the data into a single, three-dimensional volume to summarize our findings. Because of the limited number of views available, we chose to construct a simple envelope encompassing all the conformations found in the data. First, two-dimensional envelopes were generated for each of the motor domain groups (Fig.

Figure 6. Results of classification. The data were classified twice, once according to the motor domain (*top row*), and once according to the regulatory domain (*left column*). The table of images shows the subaverages of those heads allocated to each combination of motor domain and regulatory domain. The number of images belonging to each group or subgroup is indicated in the top right corner. Note the uneven distribution in the positions of the regulatory domains among different motor domain groups. Only 10 of the 20 motor domain groups showing the greatest similarity to the S1 model are shown here.

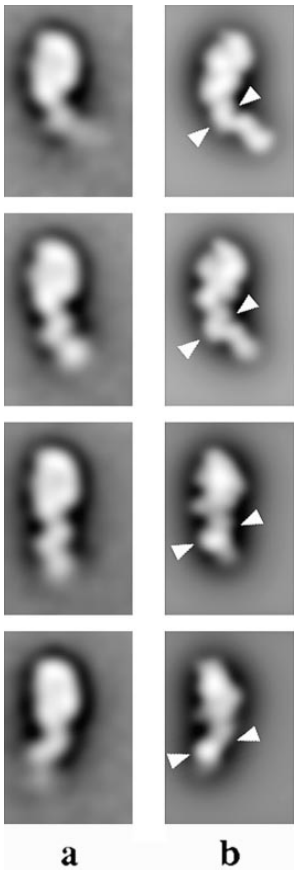

Figure 7. Comparison of the regulatory domain group averages (*a*) with the model (*b*). The model images were derived by rotating S1 about a vertical axis (in the plane of the figure) at 1° intervals and averaging them into bins of ±18°. The overall position of the regulatory domain with respect to the motor domain is consistent in all cases, as are morphological features of the regulatory domains, particularly the appearance of the essential light chains (*arrowheads*). The corresponding motor domains do not correlate as well, suggesting that the heads in our data are not rigid structures.

8 *c*). Using these and the corresponding orientations of the S1 model, we determined a three-dimensional volume using a simple back-projection method (for review see Frank, 1996). To illustrate the accuracy of the resulting envelope, it is shown projected in the same direction as each of the two-dimensional projections used in its determination (Fig. 8 *d*).

The relationship between this envelope and S1 is shown in Fig. 9. The wire frame motor domain is larger than S1, probably due to flattening during specimen preparation, but the extent of the envelope around the regulatory domain is much larger, indicating the magnitude of the movement in this part of the head. Using the S1 orientation on actin given by Whittaker et al. (1995), an imaginary actin filament would be vertical in the plane of the page in Fig. 9 *a*, and perpendicular to it in Fig. 9 *b*. Thus it can be seen that the flexibility of the regulatory domain appears to be both axial and circumferential. The maximum width of the envelope around the regulatory light chain is about 12 nm. Also, the regulatory domain of S1 lies at the periphery of this envelope rather than near its center.

Discussion

The most striking feature of the averaged head images is the amount of detail they reveal (Fig. 6). Whereas three regions were previously identified within the heads, image processing now shows considerable substructure within these regions. Classification has also enabled us to demonstrate directly that, even in the absence of nucleotide, heads display a variety of conformations.

Head Structure

The availability of the atomic structure of S1 has allowed us to construct a negative-stain model that we have used to examine the fidelity of the image averages from the micrographs. So far as we are aware, this is the first time that negatively stained, single particles have been explored in this way. The model is simple in that it includes neither stain migration (Unwin, 1974), nor positive staining (Steven and Navia, 1982), nor flattening (Seymour and De Rosier, 1987), but its similarity to the data demonstrates that the heads were exceptionally well preserved (Figs. 7 and 8). The three distinct morphological regions in the heads, reported by Walker et al. (1985) and Walker and Trinick (1988) are confirmed here (Fig. 6) and shown to correspond to the motor domain, and the essential and regulatory light chains (Figs. 7 and 8). Not only are these regions resolved in the averages, but details within them show many similarities to the model (Figs. 7 and 8). Having once seen these averages, particular details can be identified in the original micrographs (Figs. 1 and 2).

Single-particle image processing was previously applied to myosin molecules shadowed with platinum by Vibert (1988). Shadowing myosin molecules shows fewer features than negative staining, because platinum grains are substantially larger than uranyl crystallites; thus the resolution of the shadowed averages was estimated to be ~4 nm. A large distal domain was identified, but this was cusp shaped, possibly as a result of the low shadowing angle used (5°). A neck region corresponding to the regulatory domain was seen, but this was not resolved into two regions.

Head Flexibility

Each of the columns in Fig. 6 shows a constant motor domain appearance but considerable variability in the regulatory domain. This suggests strongly that there were movements between the motor and regulatory domains; however, the exact nature of this flexibility is difficult to establish. Each of the four rows in Fig. 6 has a relatively constant regulatory domain and these are similar to the appearances generated by rotating the S1 model at 36° intervals (Fig. 7). Thus it appears that some of the head flexibility can be accounted for by relative rotation of the motor and regulatory domains, but caution is necessary because the restricted size of the data set necessitated division of the heads into a small number of groups. Classification into more groups also suggested flexibility, but the regulatory domains were less similar to the group averages shown in Fig. 7 (data not shown). Thus we cannot rule out other motions such as flexing of the regulatory domain.

The average regulatory domain conformations (Fig. 8 *a*) are straighter than their modeled counterparts (Fig. 8 *b*). Thus the sharply curved conformation of S1 determined by crystallography is relatively uncommon among stained heads. This difference may occur because staining tends to straighten heads; alternatively, crystallization may impose a curved conformation on a structure that is much more mobile in solution. The extent of flexibility is such that the regulatory light chain can move by up to 12 nm in both axial and circumferential directions (Fig. 9). However, given the number of images in each of the subgroup averages (Fig. 6), the incidence of such large movements is rare.

Figure 8. Comparison with modeled S1. The 10 motor domain groups (*a*, shown also in Fig. 6) and their corresponding best matches with S1 modeled in negative stain (*b*). The motor domains in the group averages are generally larger than in the model but many features are shared. Note the difference in position of the regulatory domain in the model and the average position in each motor domain group. A two-dimensional envelope was derived for each motor domain group (*c*) encompassing all regulatory domain positions. Using these envelopes and the orientations derived from the S1 model, a simple three-dimensional envelope was calculated that, when equivalently projected, produced the images shown in *d*.

Several reports suggest that heads are capable of substantial flexibility, even when not hydrolyzing ATP. Craig et al. (1980) showed micrographs in which the heads in individual heavy meromyosin molecules curved differently when bound to adjacent actin filament subunits. Irving et al. (1995) used fluorescence polarization to show that the regulatory domain is distorted when rigor fibers are stretched, and Schmitz et al. (1996) reconstructed insect flight muscle, in which rigor heads showed a variety of conformations distinct from the S1 structure. Even in the absence of externally imposed force, the regulatory domains of frozen S1-decorated actin filaments are poorly defined (Jontes et al., 1995; Milligan and Flicker, 1987; Whittaker et al., 1995); this result was attributed to disorder, presumably resulting from Brownian motion. Such head flexibility may underlie cross-bridge compliance, as proposed by Huxley and Simmons (1971), and is probably an essential property of cross-bridges, allowing strain energy to be stored and dissipated gradually.

Head flexibility may be affected by actin binding or the presence of nucleotide and we cannot rule out effects of the staining method. Nevertheless, the present work shows directly that myosin heads are capable of substantial changes in shape, achieved by movements between the motor and regulatory domains, and such movements are consistent with the predicted properties of cross-bridges.

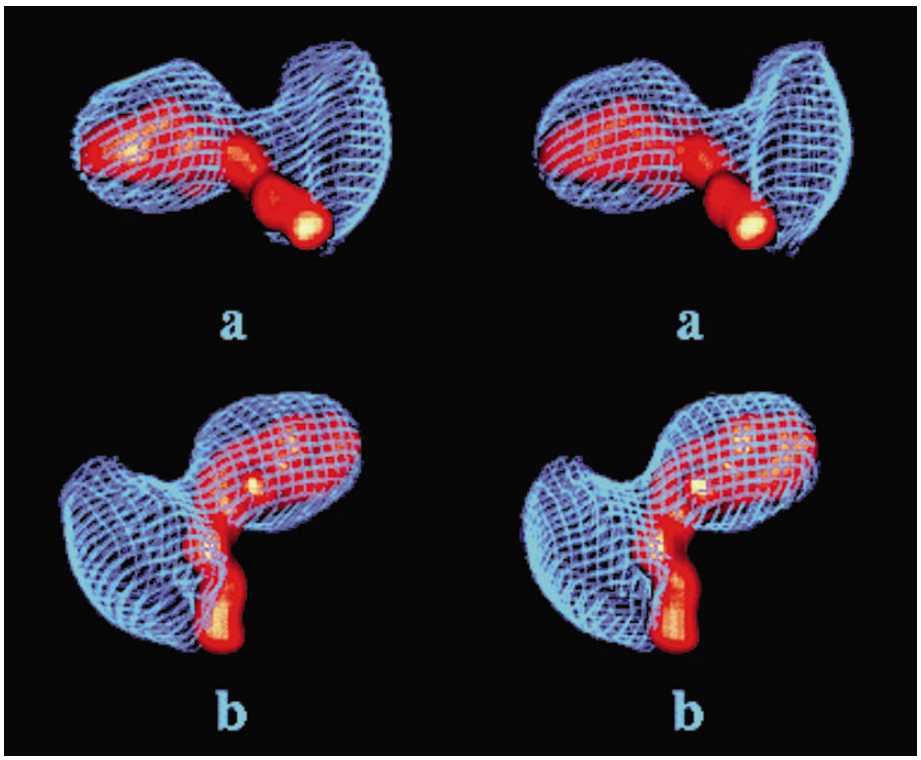

Figure 9. Stereo pair images of the S1 atomic structure (*red*) and the negative stain envelope (*blue wire mesh*), superimposed. The extent of the envelope around the regulatory domain is large compared to that around the motor domain. In the orientation shown in *a*, the actin filament would lie in the plane of the figure (see Results), and in *b* would lie perpendicular to the plane of the figure. The conformation of S1 lies at the periphery of the regulatory domain envelope, suggesting that it is rarely seen among stained heads.

We thank P. Knight and G. Offer for comments on an earlier version of the manuscript.

This work was supported by National Institutes of Health grant AR40964 and the Medical Research Council (UK).

Received for publication 30 May 1997 and in revised form 30 July 1997.

References

Craig, R., A.G. Szent-Gyorgyi, L. Beese, P. Flicker, P. Vibert, and C. Cohen. 1980. Electron microscopy of thin filaments decorated with Ca^{2+}-regulated myosin. *J. Mol. Biol.* 140:35–55.

Frank, J. 1990. Classification of macromolecular assemblies studied as "single particles." *Rev. Biophys.* 23:281–329.

Frank, J. 1996. Three-Dimensional Electron Microscopy of Macromolecular Assemblies. Academic Press, San Diego. 342 pp.

Frank, J., B. Shimkin, and H. Dowse. 1981*a.* SPIDER—a modular software system for electron image-processing. *Ultramicroscopy.* 6:343–357.

Frank, J., A. Verschoor, and M. Boublik. 1981*b.* Computer averaging of electron-micrographs of 40s ribosomal-subunits. *Science (Wash. DC).* 214:1353–1355.

Huxley, H.E. 1969. The mechanism of muscle contraction. *Science (Wash. DC).* 164:1356–1366.

Huxley, A.F., and R.M. Simmons. 1971. Proposed mechanism of force generation in striated muscle. *Nature (Lond.).* 233:533–538.

Irving, M., T. St Claire Allen, C. Sabido-David, J.S. Craik, B. Brandmeier, J. Kendrick-Jones, J.E.T. Corrie, D.R. Trentham, and Y.E. Goldman. 1995. Tilting of the light-chain region of myosin during step length changes and active force generation in skeletal muscle. *Nature (Lond.).* 375:688–691.

Jontes, J.D., E.M. Wilson-Kubalek, and R.A. Milligan. 1995. A 32-degrees tail swing in brush-border myosin-I on ADP release. *Nature (Lond.).* 378:751–753.

Milligan, R.A., and P.F. Flicker. 1987. Structural relationships of actin, myosin, and tropomyosin revealed by cryo-electron microscopy. *J. Cell Biol.* 105:29–39.

Penczek, P., M. Radermacher, and J. Frank. 1992. 3-dimensional reconstruction of single particles embedded in ice. *Ultramicroscopy.* 40:33–53.

Penczek, P.A., R.A. Grassucci, and J. Frank. 1994. The ribosome at improved resolution: new techniques for merging and orientation refinement in 3d cryo-electron microscopy of biological particles. *Ultramicroscopy.* 53:251–270.

Perry, S.V. 1955. *Methods Enzymol.* 2:582–588.

Rayment, I., H.M. Holden, M. Whittaker, C.B. Yohn, M. Lorenz, K.C. Holmes, and R.A. Milligan. 1993*a.* Structure of the actin-myosin complex and its implications for muscle contraction. *Science (Wash. DC).* 261:58–65.

Rayment, I., W.R. Rypniewski, K. Schmidtbase, R. Smith, D.R. Tomchick, M.M. Benning, D.A. Winkelmann, G. Wesenberg, and H.M. Holden. 1993*b.* 3-dimensional structure of myosin subfragment-1: a molecular motor. *Science (Wash. DC).* 261:50–58.

Schmitz, H., M.C. Reedy, M.K. Reedy, R.T. Tregear, H. Winkler, and K.A. Taylor. 1996. Electron tomography of insect flight-muscle in rigor and AMP-PNP at 23°C. *J. Mol. Biol.* 264:279–301.

Seymour, J., and D.J. DeRosier. 1987. The projection of a negatively-stained filamentous object down its central axis as revealed by image-reconstruction from tilt series. *J. Microsc. (Oxf.).* 148:195–210.

Steven, A.C., and M.A. Navia. 1982. Specificity of stain distribution in electron-micrographs of protein molecules contrasted with uranyl acetate. *J. Microsc. (Oxf.).* 128:145–155.

Unwin, P.N.T. 1974. Electron microscopy of the stacked disc aggregate of tobacco mosaic virus protein. Influence of electron irradiation on the stain distribution. *J. Mol. Biol.* 87:657–670.

Vibert, P.J. 1988. Domain structure of the myosin head in correlation-average images of shadowed molecules. *J. Muscle Res. Cell Motil.* 9:147–155.

Walker, M., and J. Trinick. 1986. Electron microscope study of the effect of temperature on the length of the tail of the myosin molecule. *J. Mol. Biol.* 192:661–667.

Walker, M., and J. Trinick. 1988. Visualization of domains in native and nucleotide-trapped myosin heads by negative staining. *J. Muscle Res. Cell Motil.* 9: 359–366.

Walker, M., P. Knight, and J. Trinick. 1985. Negative staining of myosin molecules. *J. Mol. Biol.* 184:535–542.

Whittaker, M., E.M. Wilson-Kubalek, J.E. Smith, L. Faust, R.A. Milligan, and H.L. Sweeney. 1995. A 35-Angstrom movement of smooth-muscle myosin on ADP release. *Nature (Lond.).* 378:748–751.